Proceedings of ICAR 2003
The 11th International Conference on Advanced Robotics
Coimbra, Portugal, June 30 - July 3, 2003

Fractional-Order Hybrid Control of Robotic Manipulators

N. M. Fonseca Ferreira
Dept. of Electrical Engineering
Institute of Engineering of Coimbra
Quinta da Nora
3031-601 Coimbra Codex, Portugal
email: nunomig@isec.pt

J. A. Tenreiro Machado
Dept. of Electrical Engineering
Institute of Engineering of Porto
Rua Dr António Bernardino de Almeida
4200-072 Porto Codex, Portugal
email: jtm@dee.isep.ipp.pt

Abstract

This paper presents the implementation of fractional-order algorithms in the position/force hybrid control of robotic manipulators. The system performance and robustness is analyzed in the time and frequency domains. The effect of dynamic backlash and flexibility is also investigated.

1. Introduction

In the early eighties Raibert and Craig [1] introduced the concept of force control based on the hybrid algorithm and, since then, several researchers developed those ideas and proposed other schemes [2-4].

This paper studies the position/force control of robot manipulators, required in processes that involve contact between the gripper and the environment, using fractional-order (*FO*) controllers. The application of the theory of fractional calculus is still in a research stage, but the recent progress in this area reveals promising aspects for future developments [5-10].

In this line of thought the article is organized as follows. Sections two and three introduce the position/force hybrid controller and the fundamentals of the fractional-order algorithms, respectively. Section four presents several experiments for the analysis and performance evaluation of *FO* and *PID* controllers, for robots having several types of dynamic phenomena at the joints. Finally, section five outlines the main conclusions.

2. The Hybrid Controller

The dynamical equation of a n dof robot is:

$$\boldsymbol{\tau} = \mathbf{H}(\mathbf{q})\ddot{\mathbf{q}} + \mathbf{C}(\mathbf{q},\dot{\mathbf{q}}) + \mathbf{G}(\mathbf{q}) - \mathbf{J}^{\mathbf{T}}(\mathbf{q})\mathbf{F} \tag{1}$$

where $\boldsymbol{\tau}$ is the $n \times 1$ vector of actuator torques, $\mathbf{q}$ is the $n \times 1$ vector of joint coordinates, $\mathbf{H(q)}$ is the $n \times n$ inertia matrix, $\mathbf{C}(\mathbf{q},\dot{\mathbf{q}})$ is the $n \times 1$ vector of centrifugal/Coriolis terms and $\mathbf{G(q)}$ is the $n \times 1$ vector of gravitational effects. The $n \times m$ matrix $\mathbf{J^T(q)}$ is the transpose of the Jacobian matrix of the robot and $\mathbf{F}$ is the $m \times 1$ vector of the force that the (m-dimensional) environment exerts in the robot gripper.

In this study we shall adopt as prototype manipulator the 2*R* robot (Fig. 1) with dynamics given by:

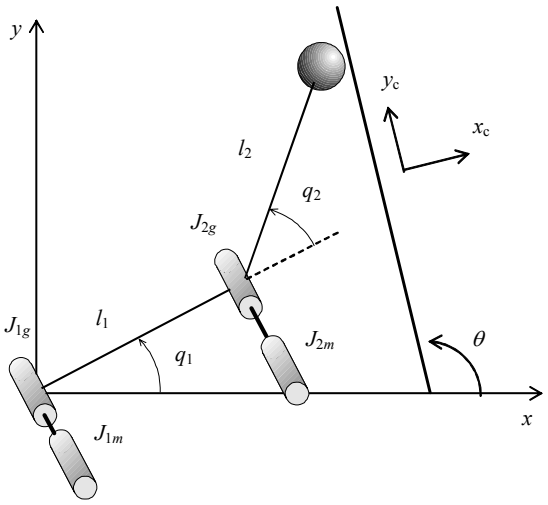

Figure 1 - The 2*R* robot and the constraint surface.

$$\mathbf{H}(\mathbf{q}) = \begin{bmatrix} (m_1+m_2)r_1^2 + m_2 r_2^2 + 2m_2 r_1 r_2 C_2 + J_{1m} + J_{1g} & m_2 r_2^2 + m_2 r_1 r_2 C_2 \\ m_2 r_2^2 + m_2 r_1 r_2 C_2 & m_2 r_2^2 + J_{2m} + J_{2g} \end{bmatrix} \tag{2a}$$

$$\mathbf{C}(\mathbf{q},\dot{\mathbf{q}}) = \begin{bmatrix} -m_2 r_1 r_2 S_2 \dot{q}_2^2 - 2m_2 r_1 r_2 S_2 \dot{q}_1 \dot{q}_2 \\ m_2 r_1 r_2 S_2 \dot{q}_1^2 \end{bmatrix} \tag{2b}$$

$$\mathbf{G}(\mathbf{q}) = \begin{bmatrix} g(m_1 r_1 C_1 + m_2 r_1 C_1 + m_2 r_2 C_{12}) \\ g m_2 r_2 C_{12} \end{bmatrix} \tag{2c}$$

$$\mathbf{J^T}(\mathbf{q}) = \begin{bmatrix} -r_1 S_1 - r_2 S_{12} & r_1 C_{11} + r_2 C_{12} \\ -r_2 S_{12} & r_2 C_{12} \end{bmatrix} \tag{2d}$$

where $C_{ij} = \cos(q_i + q_j)$ and $S_{ij} = \sin(q_i + q_j)$.

The numerical values adopted for the 2*R* robot [9] are $m_1 = 0.5$ kg, $m_2 = 6.25$ kg, $r_1 = 1.0$ m, $r_2 = 0.8$ m, $J_{1m} = J_{2m} = 1.0$ kgm^2 and $J_{1g} = J_{2g} = 4.0$ kgm^2.

The constraint plane is determined by the angle θ (Fig. 1) and the contact displacement x_c of the robot gripper with the constraint surface is modeled through a linear system with a mass M, a damping B and a stiffness K with dynamics:

$$F_c = M\ddot{x}_c + B\dot{x}_c + Kx_c \tag{3}$$

The structure of the position/force hybrid control algorithm is depicted in Fig. 2. The diagonal $n \times n$ selection matrix **S** has elements equal to one (zero) in the position (force) controlled directions and **I** is the $n \times n$ identity matrix. In this paper the y_c (x_c) cartesian coordinate is position (force) controlled, yielding:

$$\mathbf{S}=\begin{bmatrix}0 & 0\\ 0 & 1\end{bmatrix},\ \mathbf{J_c}(\mathbf{q})=\begin{bmatrix}-r_1C_{\theta 11}-r_2C_{\theta 12} & -r_2C_{\theta 12}\\ r_1S_{\theta 11}+r_2S_{\theta 12} & r_2S_{\theta 12}\end{bmatrix} \quad (4)$$

where $C_{\theta ij}=\cos(\theta-q_i-q_j)$ and $S_{\theta ij}=\sin(\theta-q_i-q_j)$.

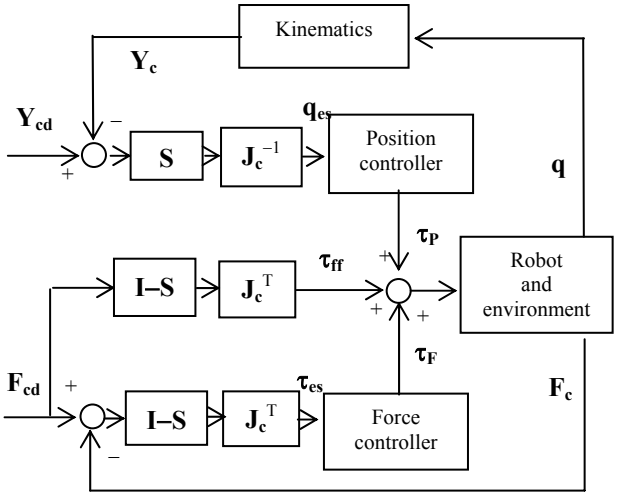

Figure 2 – The position/force hybrid controller.

3. Fractional Order Algorithms

In this section we present the *FO* controllers inserted at the position and force control loops.

The mathematical definition of a derivative of fractional order α has been the subject of several different approaches. For example, we can mention the Laplace and the Grünwald-Letnikov definitions:

$$D^{\alpha}[x(t)] = L^{-1}\{s^{\alpha}\,X(s)\} \quad (5a)$$

$$D^{\alpha}[x(t)] = \lim_{h\to 0}\left[\frac{1}{h^{\alpha}}\sum_{k=1}^{\infty}\frac{(-1)^k\Gamma(\alpha+1)}{\Gamma(k+1)\Gamma(\alpha-k+1)}x(t-kh)\right] \quad (5b)$$

where Γ is the gamma function and h is the time increment. In our case, for implementing *FO* algorithms of the type $C(s) = K\,s^{\alpha}$, we adopt a 4th-order discrete-time Pade approximation ($a_i, b_i, c_i, d_i \in \Re$, $n = 4$):

$$C_P(z) \approx K_P\,\frac{a_0z^n + a_1z^{n-1} + .. + a_n}{b_0z^n + b_1z^{n-1} + ... + b_n} \quad (6a)$$

$$C_F(z) \approx K_F\,\frac{c_0z^n + c_1z^{n-1} + .. + c_n}{d_0z^n + d_1z^{n-1} + ... + d_n} \quad (6b)$$

where K_P /K_F are the position/force loop gains.

4. Controller Performances

This section analyzes the system performance both for ideal transmissions and robots with dynamic phenomena at the joints, such as backlash and flexibility. Moreover, we compare the response of *FO* and the *PD*: $C_P(s) = K_p + K_d\,s$ and *PI*: $C_F(s) = K_p + K_i\,s^{-1}$ controllers, in the position and force loops [11-13].

Both algorithms were tuned by trial and error having in mind getting a similar performance in the two cases. The resulting parameters were *FO*: $\{K_P,\alpha_P\}\equiv\{10^5, 1/2\}$, $\{K_F,\alpha_F\}\equiv\{10^3,-1/5\}$ and *PD/PI*: $\{K_p,K_d\}\equiv\{10^4,10^3\}$, $\{K_p,K_i\}\equiv\{10^3,10^2\}$ for the position and force loops, respectively. Moreover, it is adopted the operating point $\{x,y\}\equiv\{1,1\}$, a constraint surface with parameters $\{\theta,M,B,K\}\equiv\{\pi/2,10^3,1.0,10^2\}$ and a controller sampling frequency $f_c = 1$ kHz.

In order to study the system dynamics we apply, separately, rectangular pulses, at the position and force references, that is, we perturb the references with $\{\delta y_{cd},\delta F_{cd}\} = \{10^{-1},0\}$ and $\{\delta y_{cd},\delta F_{cd}\} = \{0,10^{-1}\}$.

A. Time response

Figure 3 depicts the time response of the 2*R* robot under the action of the *FO* and the *PD/PI* controllers for ideal transmissions at the joints.

In a second phase (Fig. 4) we analyze the response of a 2*R* robot with dynamic backlash at the joints [13-14]. For the *i*th joint gear, with clearance h_i, the backlash reveals impact phenomena between the inertias, which obey the principle of conservation of momentum and the Newton law:

$$\dot{q}_i' = \frac{\dot{q}_i(J_{ii}-\varepsilon J_{im})+\dot{q}_{im}J_{im}(1+\varepsilon)}{J_{ii}+J_{im}} \quad (7a)$$

$$\dot{q}_{im}' = \frac{\dot{q}_iJ_i(1+\varepsilon)+\dot{q}_{im}(J_{im}-\varepsilon J_{ii})}{J_{ii}+J_{im}} \quad (7b)$$

where $0 \le \varepsilon \le 1$ is a constant that defines the type of impact ($\varepsilon = 0$ inelastic impact, $\varepsilon = 1$ elastic impact) and $\dot{q}_i'$ and $\dot{q}_{im}'$ are the inertias velocities of the joint and motor after the collision, respectively. The parameter J_{ii} (J_{im}) stands for the link (motor) inertias of joint *i*. The numerical values adopted are $h_i = 1.8\ 10^{-4}$ rad and $\varepsilon_i = 0.8$ ($i = 1, 2$).

In a third phase (Fig. 5) we study the 2*R* robot with compliant joints. For this case the dynamic model corresponds to model (1) augmented by the equations:

$$\boldsymbol{\tau} = \mathbf{J_m}\ddot{\mathbf{q}}_\mathbf{m} + \mathbf{B_m}\dot{\mathbf{q}}_\mathbf{m} + \mathbf{K_m}(\mathbf{q_m}-\mathbf{q}) \quad (8a)$$

$$\mathbf{K_m}(\mathbf{q_m}-\mathbf{q}) = \mathbf{J}(\mathbf{q})\ddot{\mathbf{q}} + \mathbf{C}(\mathbf{q},\dot{\mathbf{q}}) + \mathbf{G}(\mathbf{q}) \quad (8b)$$

where $\mathbf{J_m}$, $\mathbf{B_m}$ and $\mathbf{K_m}$ are the $n \times n$ diagonal matrices of the motor and transmission inertias, damping and stiffness, respectively. In the simulations we adopt $K_{mi} = 2\ 10^6$ Nm rad^{-1} and $B_{mi} = 10^4$ Nms rad^{-1} ($i = 1,2$).

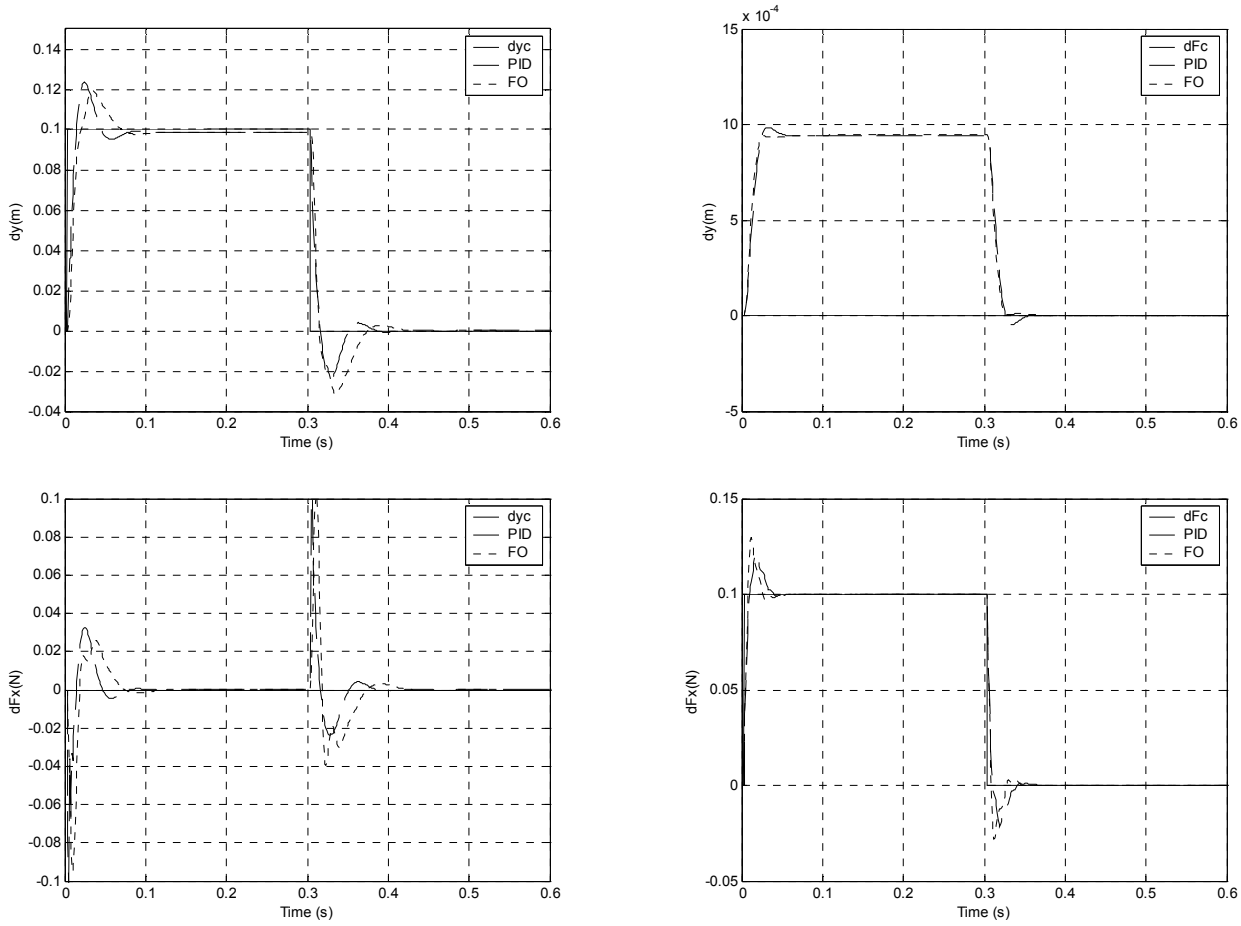

Figure 3 – Time response for the 2*R* ideal robot under the action of the *FO* and *PD/PI* controllers.

Table I – The time response parameters for a rectangular pulse δy_{cd} at the position reference.

joint		*PO%*	e_{ss}	T_p	T_s
ideal	*PID*	23.48%	$99\ 10^{-3}$	0.122	0.013
	FO	18.98%	$79\ 10^{-3}$	0.033	0.018
backlash	*PID*	0.37%	$2.1\ 10^{-3}$	0.383	0.080
	FO	0.36%	$1.4\ 10^{-4}$	0.302	0.118
flexible	*PID*	2.28%	$3.9\ 10^{-3}$	0.403	1.502
	FO	1.80%	$1.4\ 10^{-3}$	0.302	3.004

Table II – The time response parameters for rectangular pulse δFcd at the force reference.

joint		*PO%*	e_{ss}	T_p	T_s
ideal	*PID*	22.04%	$1.3\ 10^{-3}$	0.083	0.091
	FO	29.54%	$1.3\ 10^{-3}$	0.089	0.093
backlash	*PID*	5.98%	$9.9\ 10^{-2}$	0.402	0.405
	FO	0.86%	$9.9\ 10^{-2}$	0.079	0.043
flexible	*PID*	3.28%	$9.9\ 10^{-2}$	0.602	0.602
	FO	1.82%	$9.9\ 10^{-2}$	0.450	0.450

The time responses (Tables I and II), namely the percent overshoot *PO%*, the steady-state error e_{ss}, the peak time T_p and the settling time T_s, reveal that, although tuned for similar performances in the first case, the *FO* is superior to the *PD/PI* in the cases with dynamical phenomena at the robot joints.

B. Frequency response

Figures 6-7 show the transfer functions $|Y_c(j\omega)/Y_{cd}(j\omega)|$, $|F_c(j\omega)/F_{cd}(j\omega)|$, $|Y_c(j\omega)/F_{cd}(j\omega)|$ and $|F_c(j\omega)/Y_{cd}(j\omega)|$ (where $Y_c(j\omega)=F\{\delta y_c\}$ and $F_c(j\omega)=F\{\delta F_c\}$) for the *FO* and the *PD/PI* controllers, in the cases of an ideal robot and a robot with flexibility at the joints, respectively.

The low-pass characteristics of $|Y_c(j\omega)/Y_{cd}(j\omega)|$ and $|F_c(j\omega)/F_{cd}(j\omega)|$ have a cut-off frequency that depends on the environment parameters. On the other hand, $|Y_c(j\omega)/F_{cd}(j\omega)|$ and $|F_c(j\omega)/Y_{cd}(j\omega)|$ reveal the existence of some coupling between the position and force loops due to the non-ideal performance of both algorithms. Furthermore, in the case of flexibility we observe a resonance peak for $\omega \approx 5.0\ 10^2$ rad s^{-1}.

In order to compare the robustness of both algorithms, for a variation of constraints surface parameters, we consider the cases $M\equiv\{10^{-4}, 10^{-3}, 10^{-2}\}$, $B\equiv\{0.5, 1.0, 2.0\}$ and $K\equiv\{10,\ 10^2,\ 2\ 10^2\}$. Figures 8-10 depicts the corresponding frequency responses $|Y_c(j\omega)/Y_{cd}(j\omega)|$ and $|F_c(j\omega)/F_{cd}(j\omega)|$.

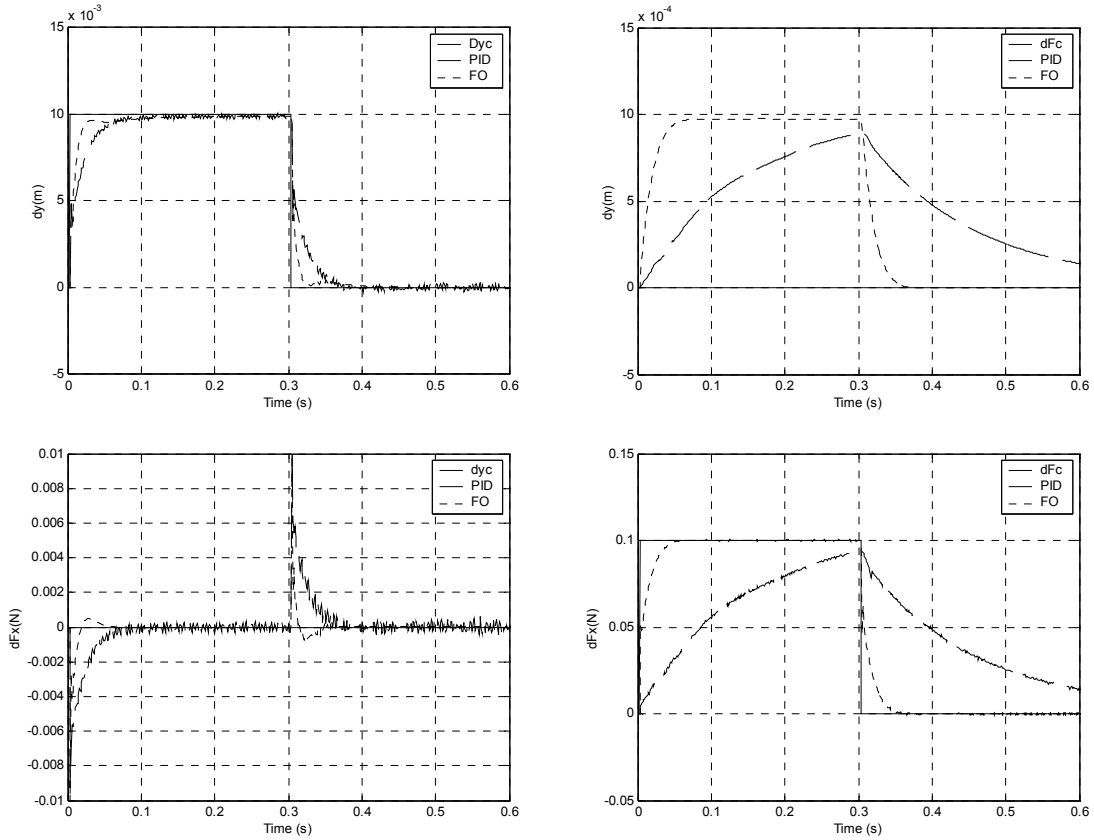

Figure 4 – Time response for the 2*R* robot with dynamic backlash under the action of the *FO* and *PD/PI* controllers.

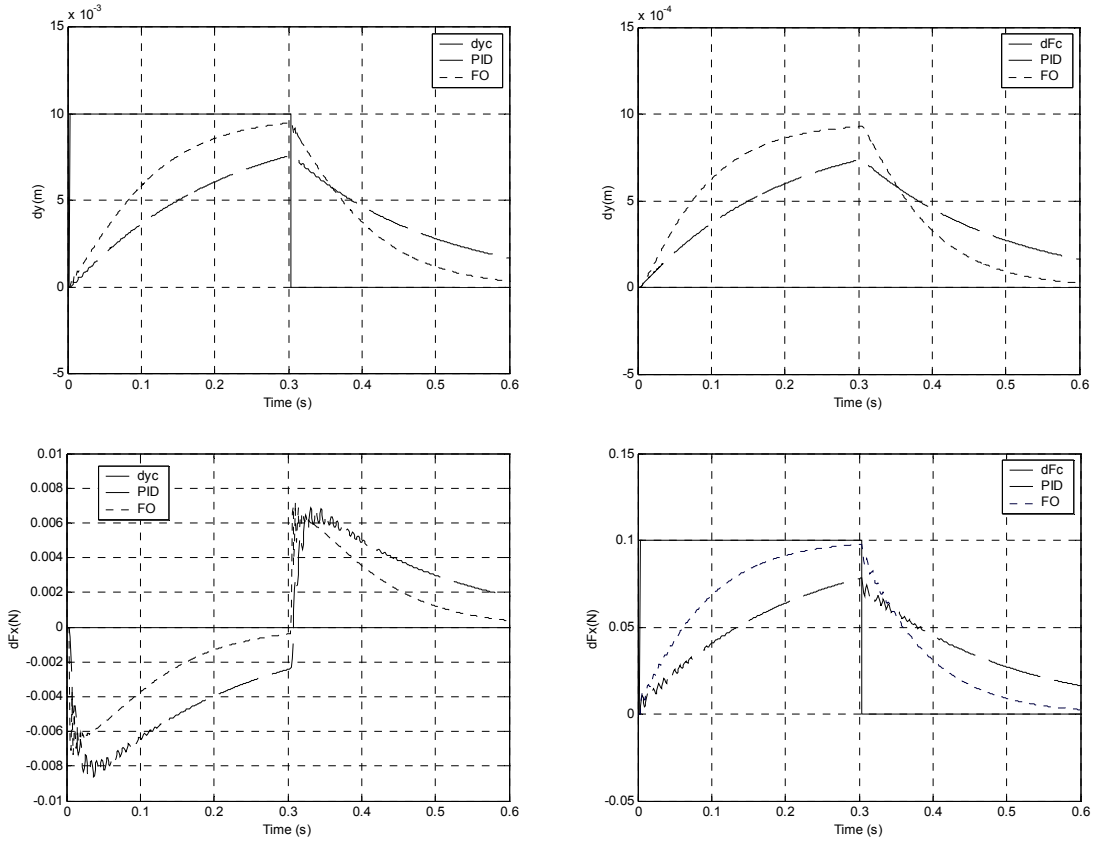

Figure 5 – Time response for the 2*R* robot with flexible joints under the action of the *FO* and *PD/PI* controllers.

5. Summary and Conclusions

This paper presented the implementation of hybrid controllers for manipulators with several types of nonlinear phenomena at the joints. The system was tested both for fractional and integer order control algorithms. The results revealed that the fractional-order algorithms have superior performances.

References

[1] M. H. Raibert and J. J. Craig, "Hybrid Position/Force Control of Manipulators", *ASME Journal of Dynamic Systems, Measurement, and Control*, vol. 102, no. 2, pp. 126–133, 1981.

[2] O. Khatib, "A Unified Approach for Motion and Force Control of Robot Manipulators: The Operational Space Formulation", *IEEE Journal of Robotics and Automation*, vol. 3, no. 1, pp. 43–53, 1987.

[3] B. Siciliano and L. Villani, "A Force/Position Regulator for Robot Manipulators without Velocity Measurements", *IEEE Int. Conf. on Robotics and Automation*, USA, 1996.

[4] A. Oustaloup, *La Commande CRONE: Commande Robuste d'Ordre Non Entier*, Hermes, 1991.

[5] A. Oustaloup, *La Dérivation Non Entière: Théorie, Synthèse et Applications*, Hermes, Paris, 1995.

[6] J. Tenreiro Machado, "Analysis and Design of Fractional-Order Digital Control Systems", *J. Systems Analysis, Modelling and Simulation*, vol. 27, pp. 107–122, 1997.

[7] J. Tenreiro Machado, A. Azenha "Fractional-Order Hybrid Control of Robot Manipulators*" IEEE Int. Conf. on Systems, Man and Cybernetics*, pp. 788–793, 1998.

[8] I. Podlubny, "Fractional-Order Systems and $PI^{\lambda}D^{\mu}$-Controllers", *IEEE Transactions on Automatic Control*, vol. 44, no. 1, pp. 208–213, 1999.

[9] S. Dubowsky, J. F. Deck and H. Costello, "The Dynamic Modelling of Flexible Spatial Machine Systems with Clearance Connections", *ASME Journal of Mechanisms, Transmissions and Automation in Design,* vol. 109, no. 1, pp. 87–94, 1987.

[10] Y. Stepanenko and T. S. Sankar, "Vibro-Impact Analysis of Control Systems with Mechanical Clearance and Its Application to Robotic Actuators", *ASME Journal of Dynamic Systems, Measurement and Control*, vol. 108, no. 1, pp. 9–16, 1986.

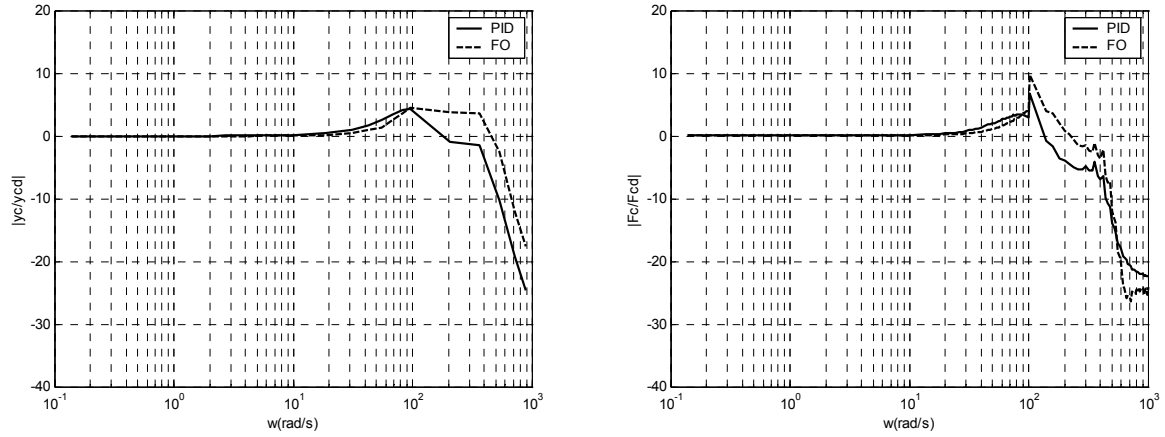

Figure 6 – Frequency responses for the 2*R* ideal robot under the action of the *FO* and *PD/PI* controllers.

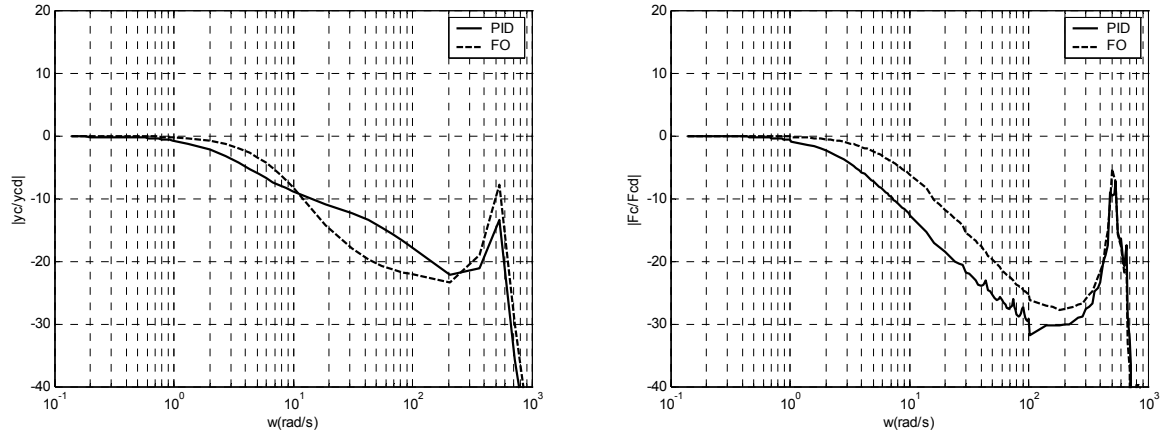

Figure 7 – Frequency responses for the 2*R* robot with flexible joints under the action of the *FO* and *PD/PI* controllers.

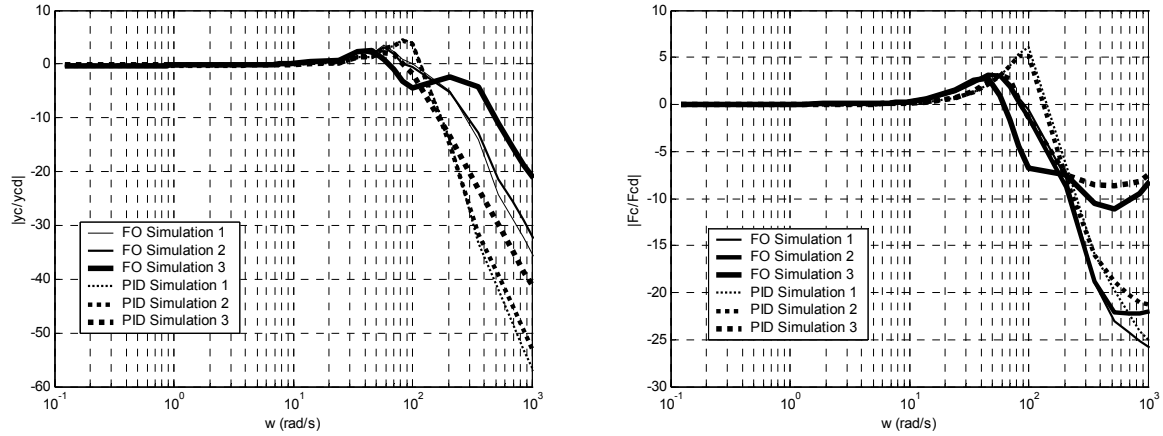

Figure 8 – Frequency responses for the 2*R* ideal robot under the action of the *FO* and *PD/PI* controllers for different surface parameters $M \equiv \{10^{-4}, 10^{-3}, 10^{-2}\}$ (simulations 1, 2 and 3).

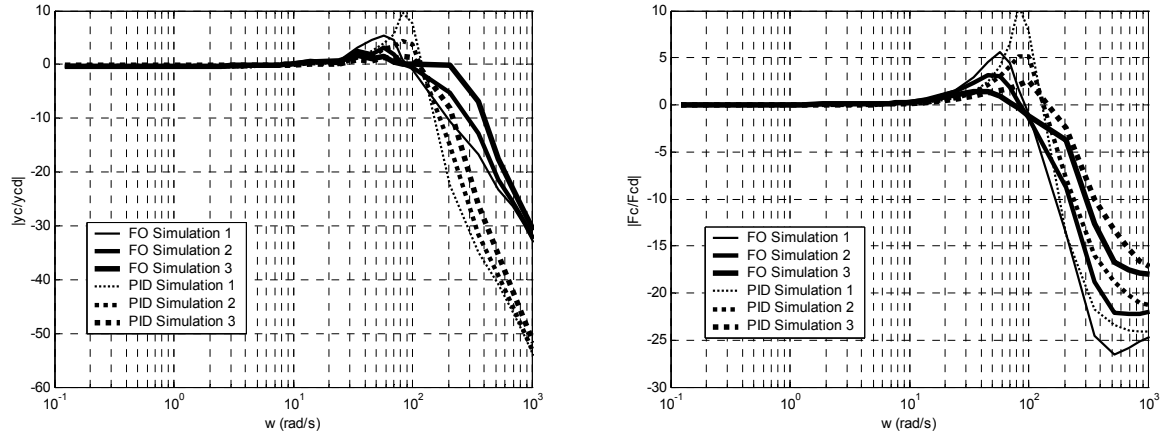

Figure 9 – Frequency responses for the 2*R* ideal robot under the action of the *FO* and *PD/PI* controllers for different surface parameters $B \equiv \{0.5, 1.0, 2.0\}$ (simulations 1, 2 and 3).

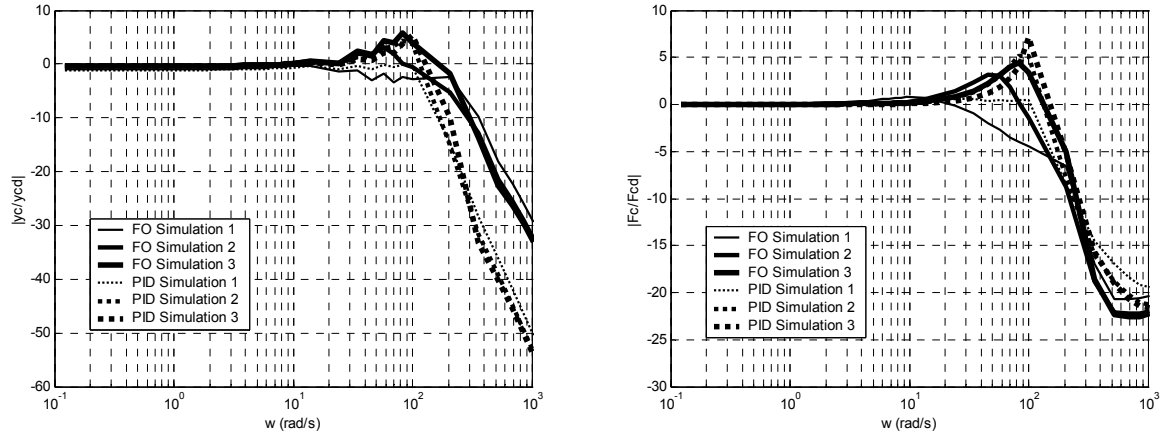

Figure 10 – Frequency responses for the 2*R* ideal robot under the action of the *FO* and *PD/PI* controllers for different surface parameters $K \equiv \{10, 10^2, 2\ 10^2\}$ (simulations 1, 2 and 3).